Observation the melting process of the phase change material inside a half-cylindrical with thermal non-equilibrium porous media: CFD simulation

Yan Cao [a], Hamdi Ayed [b], Hussein Togun [c,d,*], Hajar Alias [c], Souhail Mohamed Bouzgarrou [e,f], Makatar Wae-hayee [g,**], Riadh Marzouki [h]

[a] *School of Mechatronic Engineering, Xi'an Technological University, Xi'an, 710021, China*
[b] *Department of Civil Engineering, College of Engineering, King Khalid University, Abha, 61421, Saudi Arabia*
[c] *School of Chemical and Energy Engineering, Faculty of Engineering, University Teknologi Malaysia, 81310, UTM, Johor Bahru, Malaysia*
[d] *Biomedical Engineering Department, University of Thi-Qar, 64001, Nassiriya, Iraq*
[e] *Department of Civil Engineering, Faculty of Engineering, Jazan University, Saudi Arabia*
[f] *Higher Institute of Applied Sciences and Technology of Sousse, Sousse University, Tunisia*
[g] *Department of Mechanical and Mechatronics Engineering, Faculty of Engineering, Prince of Songkla University, Hatyai, Songkhla, 90110, Thailand*
[h] *Department of Chemistry, College of Science, King Khalid University, Abha, 61421, Saudi Arabia*

A R T I C L E   I N F O

Keywords:
Computational fluid dynamic
Phase change material
Local thermal non-equilibrium porous media
Buoyant force
Darcy model

A B S T R A C T

The aim of this study is numerically to investigate the effects of local thermal non-equilibrium porous media on the melting process of paraffin with the melting temperature $33°C$. The geometry consists of a half-cylinder containing paraffin with a uniform constant temperature and an insulating wall. Also, Darcy model and buoyant force due to density changes are considered in this simulation. The effects of the presence of aluminum foam with porosity $\varepsilon = 0.8$, *and* 0.95 and difference temperature $\Delta T = 5, 10,$ *and* 15 have been studied on the melting fraction of PCM, temperature and streamlines contours and heat flux of cylinder's surface. The observations show that enhancement of porosity 0.8 to 0.9 increases the volume of PCM 11.7%, and reduces time of melting process 30.8% for $\Delta T = 15$. Moreover, increment of $\Delta T = 5 \, to \, 15$ leads to decrease time of melting process 71.8% when porosity is 0.95.

1. Introduction

Storing energy using phase change materials is a great innovation in energy storage. These materials due to receiving and storing heat as latent heat at a constant temperature have highly regarded by researchers [1–3]. Energy storage in the form of heat at different temperatures has led to have significant applications of PCM in various industries such as cooking [4], clothing [5], textile [6], building [7–9], heating and cooling systems [10–12], desalination systems [54–56], and medicine [13].

The latent heat of PCM in solid to vapor phase is more than solid to liquid phase, but phase change solid-liquid is widely used due to low change volume [14]. Two important parameters in PCMs are latent heat and solid to liquid phase transition temperature. PCMs can

Nomenclature

A_{sf}	Surface area density, $[m^2]$
C	Specific heat capacity, $[J\ kg^{-1}\ K^{-1}]$
d_p	Pore diameter, $[m]$
d_f	Fiber diameter, $[m]$
R	Radius of cylinder, $[m]$
g	Gravitational acceleration, $[m\ s^{-2}]$
h_{sf}	Local heat transfer coefficient, $[W\ m^{-2}\ K^{-1}]$
K	Permeability, $[m^{-2}]$
k	Thermal conductivity, $[W\ m^{-1}\ K^{-1}]$
L	Latent heat, $[J\ kg^{-1}]$
P	Pressure, $[N\ m^{-2}]$
T	Temperature, $[K]$
T_M	Melting temperature, $[K]$
V	Velocity vector, $[m\ s^{-1}]$
x, y	Cartesian coordinates, $[m]$

Greek symbols

β	Thermal expansion coefficient, $[K^{-1}]$
ω	pore density, $[-]$
μ	Dynamic viscosity, $[kg\ m^{-1}\ s^{-1}]$
λ	Melting fraction, $[-]$
ρ	Density, $[kg\ m^{-3}]$
ε	Porosity, $[-]$
Re	Reynolds number
Pr	Prandtl number

Subscript

Ave	Average
C	Cold
pcm	Phase change material
f	fluid
s	Porous media

be classified into three types: organic, inorganic and eutectic mixtures. On the other hand, PCMs can be classified in approach of melting temperature (T_m) and latent heat solid-liquid (h_{sl}) as follows [15–17]:

- Queues salt solution for $-70 < T_m < 0°C$ with $220 < h_{sl} < 320\ kj/_{kg}$.
- Paraffins for $0 < T_m < 130°C$ with $180 < h_{sl} < 220\ kj/_{kg}$.
- Sugar alcohols for $60 < T_m < 210°C$ with $210 < h_{sl} < 430\ kj/_{kg}$.

Paraffins are a type of organic PCM that have more advantages such as: availability, high latent heat in solid-liquid transition, auto-nucleation properties, high nucleation rate, chemical stability, and low cost. One of the important advantages of paraffin is the melting temperature range of 0–130°, which has a very good temperature range for most industrial applications. But one of the disadvantages of paraffins is low thermal conductivity, which studies [15,18,19] have used for thermal energy storage systems, cooling photovoltaic panels, controlling temperature of medicine in delivery processes.

Residential, office and industrial buildings need a lot of energy for heating and cooling. It can be said that cooling and heating of buildings consume energy between 18 and 73% of the total energy [20] that range of energy consumption of buildings function of many different parameters such as weather conditions, geography, season, design and the used materials in the building, etc. [21–23]. One of the important applications of PCM is for cooling and heating systems of buildings. These materials are used as intelligent material to control the temperature's building. because these materials change phase at a constant temperature and response to the environmental turbulent conditions from temperature point of view and the whole process occurs at a constant temperature [24]. There are many renewable energy sources available to humans who have been able to use these resources in different ways [25–27]. It can be said that Solar energy is a remarkable renewable heat source whose heat is available worldwide. There are many ways to use solar heat. Therefore, using solar energy to melt PCM materials can be a very good option [28–30].

There are various methods for solving fluid kinematic problems and heat transfer processes such as analytical, laboratory and numerical methods. In the numerical method, the governing equations of Navier-Stokes are discretized and solved [31–33]. One of the
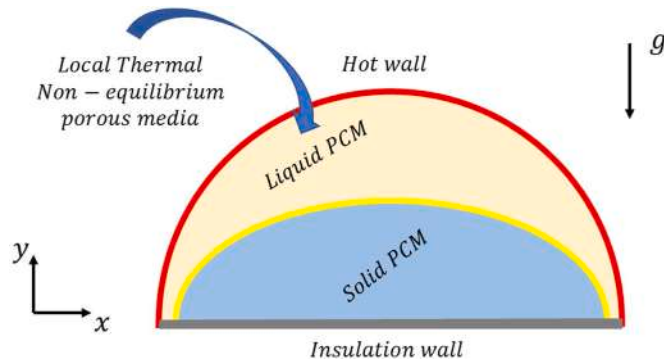
Fig. 1. A half-cylinder filled aluminum foam as porous media and paraffin as phase change material.

Table 1
The thermophysical properties of used material [57,59].

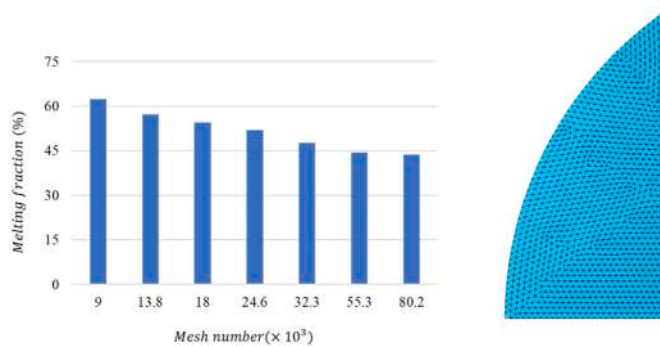| Properties	Paraffin	Aluminum foam
Density $(\frac{kg}{m^3})$	800	2700
Thermal conductivity $(\frac{W}{mK})$	0.2	205
Specific heat $(\frac{J}{kgK})$	1250	897
Viscosity $(\frac{kg}{ms})$	0.008	-
Latent heat of fusion $(\frac{J}{kgK})$	125000	-
Melting temperature (°C)	30	-
Melting temperature range (°C)	1	-
Thermal expansion coefficient $(\frac{1}{K})$	0.002	2.22×10^{-5}

Fig. 2. The mesh independence for melting fraction and a section of used unstructured mesh for current unsteady simulation.

new applications of Navier-Stokes complex equations is in simulating blood flow in the arteries [34–36] and drug delivery and drug release in the body [37–40].

Due to the widespread use of PCM, many studies have conducted on the PCM melting process using numerical methods and simulations by computational fluid dynamics (CFD) [41–43]. Badiei et al. [44] simulated the PCM melting to improve the performance of a solar flat panel collector. They used four types of PCM to have four different melting temperatures in their simulations. Their results show that the collector efficiency is improved 13% for low melting temperatures. In another numerical study by Gómez et al. [45], they simulated the effects of PCM within a wall to be fixed temperature's room versus climate changes. observations say that the wall filled PCM leads to keep the room at temperature constant and reduce the energy consumption of the cooling system. Study [46] has numerically investigated the PCM melting process in presence of a copper porous media inside rectangle chamber. They have also implemented the local thermal non-equilibrium model with enthalpy-porous method in their governing equations and studied the effects of porous media on the melting process, temperature and streamlines contours. Heat transfer phenomena in different systems have been reviewed by many researchers [47–49]. Also, using solar energy [60] is a great idea for melting phase change material, because solar energy is available both on and out the earth, as well as clean and renewable energy [50–53].
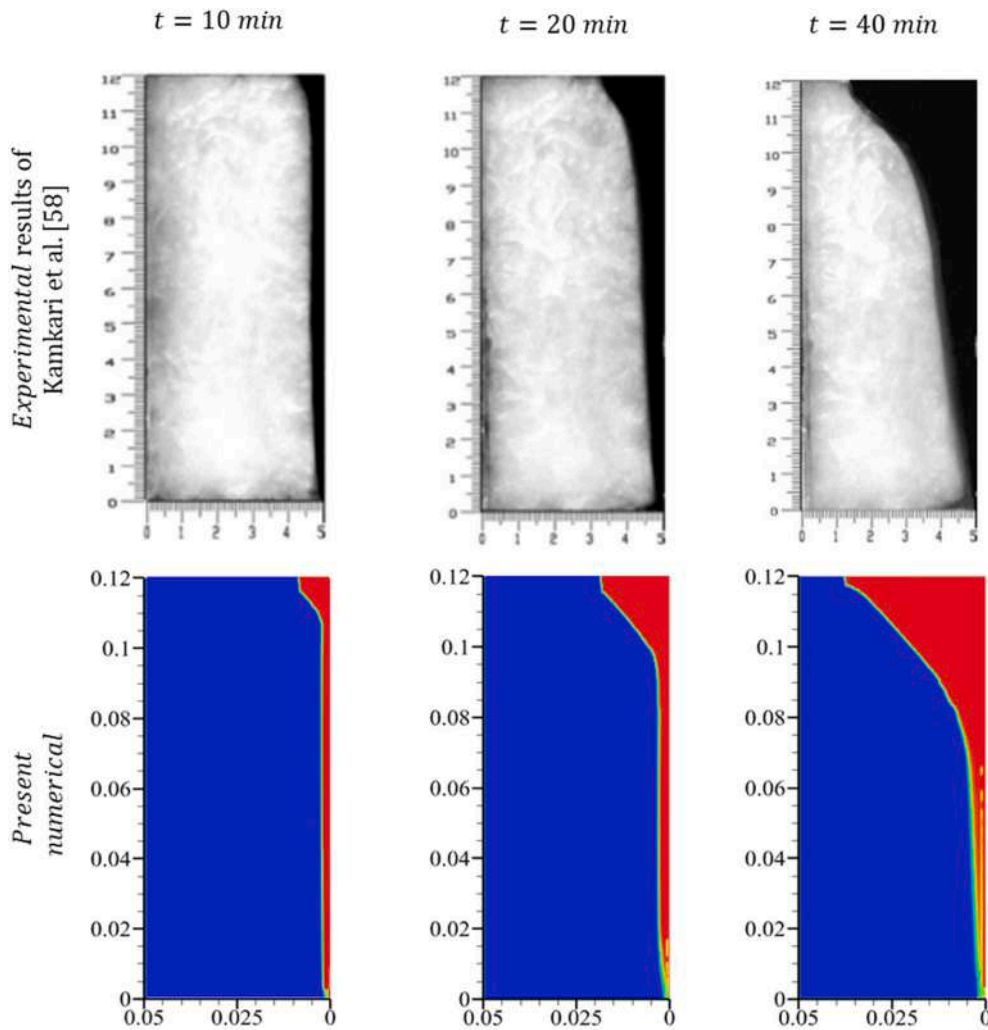
Fig. 3. Comparison of melting fraction between results of current work and Kamkari et al. [58].

As mentioned in the introduction, phase change materials are very useful for the building industry. and few studies have been simulated PCM melting process in presence of local thermal non-equilibrium porous media and has not been considered porosity on melting process with different difference temperature. In this study, the aluminum foam is embedded inside a half-cylinder with a hot wall as constant temperature for melting PCM. On the other hand, the porous medium is considered as local thermal non-equilibrium and the effects of natural convection of liquid PCM is used in governing equation in order to precise the simulation results with laboratory and physical results.

2. Geometry

The geometry consists of a porous half-cylinder with radius R = 5 cm filled paraffin as the phase change material with melting temperature $T_m = 33°C$ (see Fig. 1). The material of the porous medium is aluminum foam, which in the present simulation is investigated as local thermal non-equilibrium. It should also be noted that the top wall of the geometry is exposed by uniform constant temperature and the bottom wall is insulated. Therefore, the hot wall causes to melt the paraffin, which creates a natural convection flow inside the chamber and helps the paraffin for melting more. Note that the gravitational acceleration is $9.8 \frac{m}{s^2}$ in - y-direction.

3. Mathematical model and properties

Assumptions include two-dimensional flow, incompressible, unsteady, laminar, local thermal non-equilibrium in porous media, and constant properties. The effects of Darcy and buoyant force are considered in momentum equation due to presence of porous media and changing density with temperature, respectively. The momentum, energy equations of fluid and porous media for local thermal non-equilibrium model are represented as follows [59]:
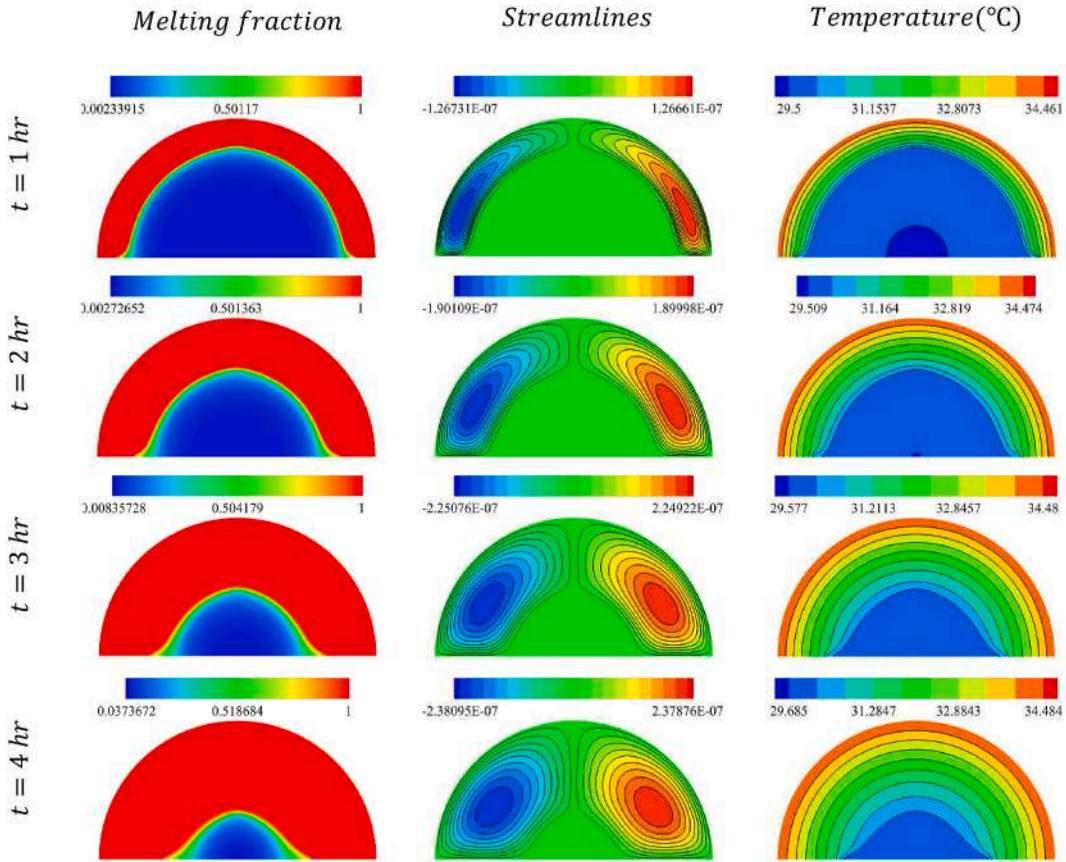
Fig. 4. The melting fraction, streamlines, temperature contours versus time for $\Delta T = 5$, $\varepsilon = 0.8$.

Momentum equation:

$$\frac{\rho_f}{\varepsilon}\frac{\partial \boldsymbol{V}}{\partial t} + \frac{\rho_f}{\varepsilon^2}(\boldsymbol{V}.\nabla)\boldsymbol{V} = -\nabla P + \frac{\mu_f}{\varepsilon}\nabla.(\nabla \boldsymbol{V}) - \frac{\mu_f}{K}\boldsymbol{V} + (\rho\beta)_f\left(T - T_{Ref}\right)\boldsymbol{g} - 10^5\frac{(1-\lambda)^2}{\lambda^3 + 0.001}\boldsymbol{V} \tag{1}$$

Which the last term of the momentum equation in right hand is the mushy term source which acts as a porous medium in the melting and solidification processes. This term indicates where PCM is in the solid phase (which is function of λ), the velocity value should be zero.

Energy equation of fluid:

$$\varepsilon\rho_f\left(C_f + L\frac{d\lambda}{dT_f}\right)\frac{\partial T_f}{\partial t} + \rho_f C_f\left(\boldsymbol{V}.\nabla T_f\right) = \varepsilon k_f \nabla.\left(\nabla T_f\right) - h_{sf}A_{sf}\left(T_f - T_s\right) \tag{2}$$

Energy equation of porous media:

$$(1-\varepsilon)\rho_s C_s\frac{\partial T_s}{\partial t} = (1-\varepsilon)k_s\nabla.(\nabla T_s) - h_{sf}A_{sf}\left(T_s - T_f\right) \tag{3}$$

The solid to fluid phase change is a function of the error function, which is calculated as follows:

$$\lambda = 0.5\ erf\left(4\frac{T_s - T_m}{T_l - T_s}\right) + 0.5 \tag{4}$$

The porous media equations can be listed as follows [57]:

$$\text{Pore diameter}\ \ d_p = \frac{0.0254}{\omega} \tag{5}$$

$$\text{Fiber diameter}\ \ \ d_f = 1.18d_p\left(\frac{1-\varepsilon}{3\pi}\right)^{1/2}\left(1 - e^{\frac{\varepsilon-1}{0.04}}\right)^{-1} \tag{6}$$
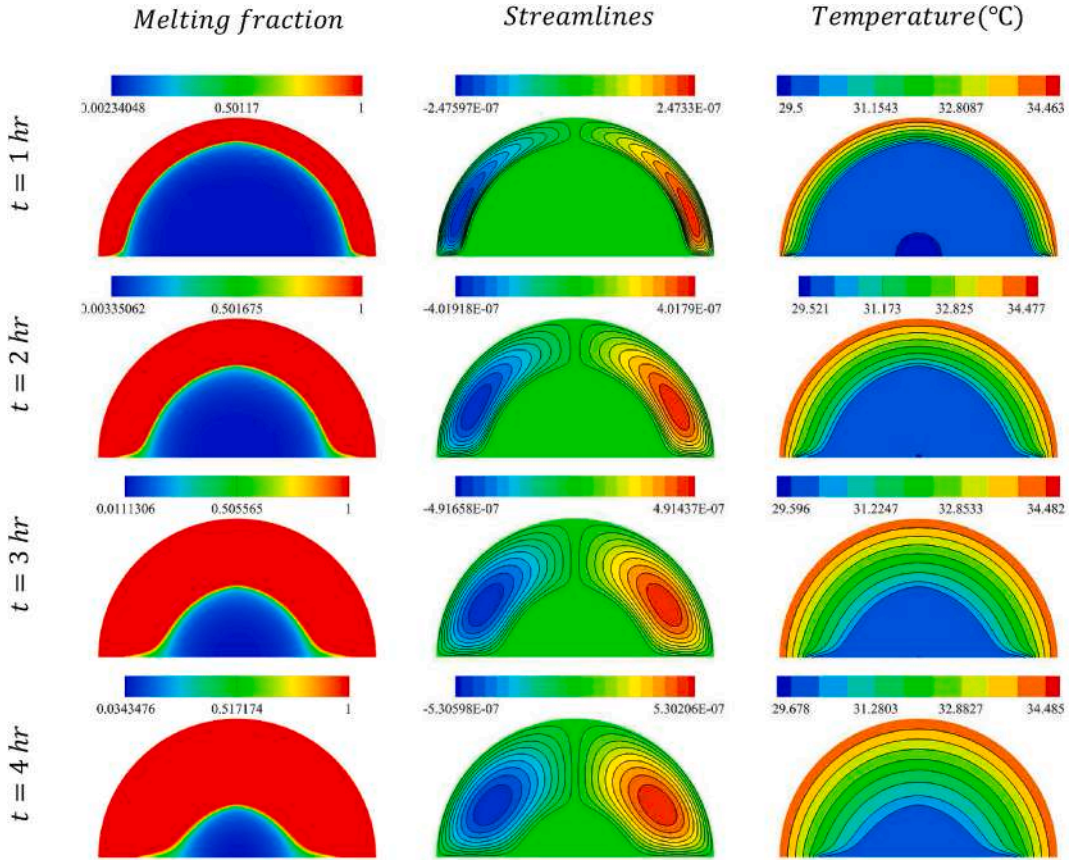
5

Fig. 5. The melting fraction, streamlines, temperature contours versus time for $\Delta T = 5$, $\varepsilon = 0.95$.

Permeability $K = 0.00073(1 - \varepsilon)^{-0.224} \left(\dfrac{d_f}{d_p} \right)^{-1.11} d_p{}^2$ (7)

Local heat transfer coefficient $h_{sf} = \begin{cases} 0.76 \left(\dfrac{k_f}{d} \right) Re_d^{0.4} Pr_{pcm}^{0.37} \ 1 \leq Re_d < 40 \\[2mm] 0.52 \left(\dfrac{k_f}{d} \right) Re_d^{0.5} Pr_{pcm}^{0.37} \ 40 \leq Re_d < 10^3 \\[2mm] 0.26 \left(\dfrac{k_f}{d} \right) Re_d^{0.6} Pr_{pcm}^{0.37} \ 10^3 \leq Re_d < 2 \times 10^5 \end{cases}$, $\begin{cases} d = d_f \left(1 - e^{\frac{\varepsilon-1}{0.04}} \right) \\[2mm] Re_d = \dfrac{\rho_f |V| d}{\mu_f} \\[2mm] Pr_{pcm} = \dfrac{\mu_f C_f}{k_f} \end{cases}$ (8)

Surface area density $A_{sf} = 3\pi d_f \left(1 - e^{\frac{\varepsilon-1}{0.04}} \right) (0.59 d_p)^{-2}$ (9)

According to the study [57], the pore density (ω) of the Aluminum foam and the is equal to 10. Moreover, Table 1 shows the thermophysical properties of paraffin and aluminum foam [57,59].

The boundary and initial conditions are required to solve the mentioned PDE equations. The geometry is at an initial temperature of $29.5°C$ (temperature of melting point) and the top wall of the geometry is at a uniform constant temperature (T_H) and the bottom wall is insulated. The non-slip condition is also used for velocity on the walls.

4. Numerical considerations

The mentioned equations are discretized by finite volume method (FVM) and solved instantaneously by PIMPLE algorithm. The PIMPLE algorithm is combinated of PISO (Pressure Implicit with Splitting of Operator) and SIMPLE (Semi-Implicit Method for Pressure-Linked Equations) algorithms. Euler, First-order upwind and Central schemes are implemented for time, convective and conductive terms, respectively. It can also be mentioned that unstructured mesh is used to simulate PCM inside the half-cylinder chamber (see Fig. 2). The mesh independence with a constant time step (1.2 s) has been checked for melting fraction in the
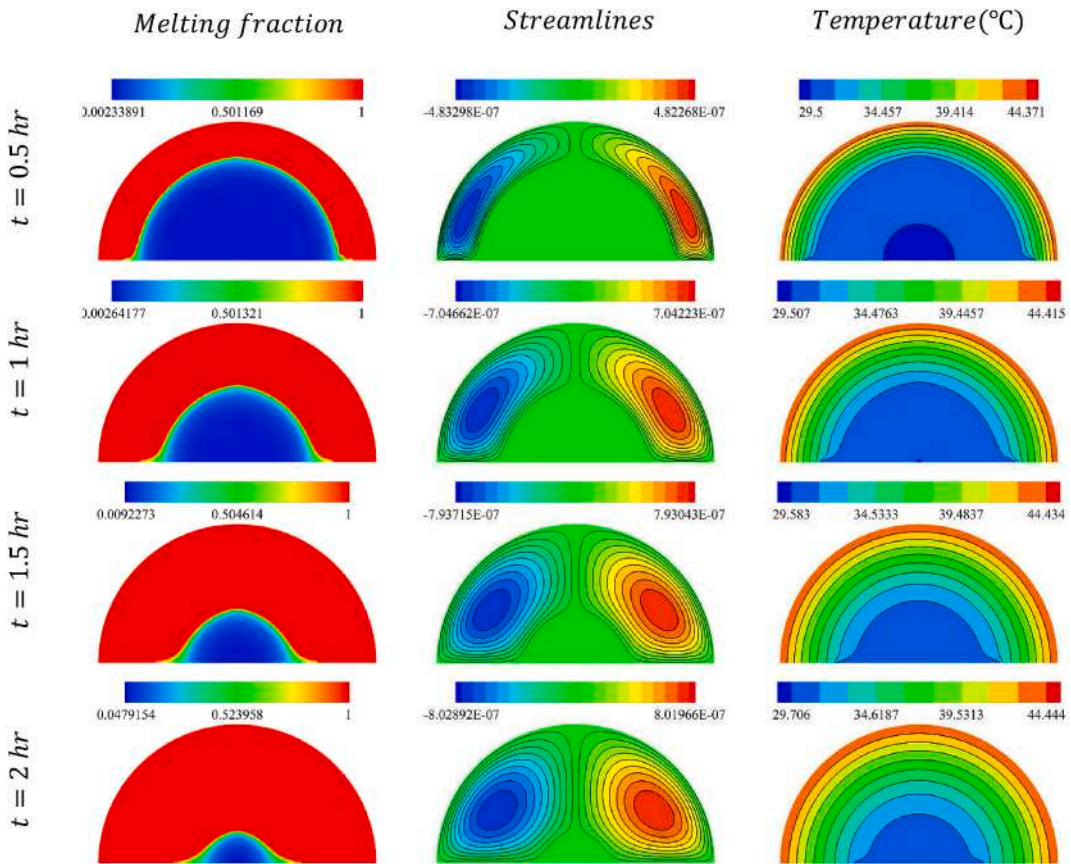
Fig. 6. The melting fraction, streamlines, temperature contours versus time for $\Delta T = 15$, $\varepsilon = 0.8$.

conditions of $\varepsilon = 0.95$, *and* $\Delta T = 10$, which in all cases the Courant number is much smaller than one. Fig. 2 demonstrates the melting fraction of paraffin for 1 h after beginning of process. the mesh 55.3k is chosen to simulate all the other cases, which the Courant number is much smaller than unit for all cases.

Kamkari et al. [58] have experimentally investigated the melting process of lauric acid as PCM in a rectangular chamber. One of a chamber walls was at a constant temperature of $70°C°C$ and the other walls were insulated and they took pictures of the melting process. Fig. 3 shows the results of the melting process of the present simulation and experimental study [58] to verify the present numerical solution. According to Fig. 3, the current results are consistent with the experimental results.

5. Results and discussions

This section investigates melting process of paraffin with melting temperature $30°C$ inside a half-cylinder in presence of thermal non-equilibrium porous media. The temperature of PCM, flow pattern, melting fraction contours, plot of melting fraction and input heat transfer rate versus time are studies for two porosity $\varepsilon = 0.8$, 0.95 and three temperature difference between top wall and melting temperature $\Delta T = 5$, 10, *and* 15.

Figs. 4 and 5 demonstrate the melting fraction, streamline and temperature contours for $\Delta T = 5$ when $\varepsilon = 0.8$, 0.95, respectively. For both porosities, after 1 h from the beginning of the melting process, the molten PCM moves due to the buoyant force, which leads to the form two clockwise and counterclockwise vortices in both sides of geometry. On the other hand, most isothermals are observed in the liquid phase region, because input heat from top wall causes to heat liquid phase as sensible heat (increment of the liquid phase temperature) and melt solid phase as latent heat.

Over time, more volume of PCM melt, which vortices become larger and stronger. Also, the center of the vortices move against gravity direction. Moreover, the isothermals are spaced apart in order to be increased the distance between the top wall and the surface of solid phase in constant temperature difference.

By comparing the two Figs. 4 and 5 at a fixed time, it can be noted that the enhancement of porosity has led to decreased melting fraction. Because the volume of PCM for a porosity 0.95 is more than porosity 0.8. On the other hand, the strength of streamlines has been increased by rising porosity because resistance of the porous medium has been reduced versus movement of the fluid flow. In addition, the isothermals for both porosities are similar except at the bottom of the chamber where the density of isothermals is high.

The mentioned arguments for Figs. 4 and 5 at a fixed porosity are true to Figs. 6 and 7. But there are many differences, which will be
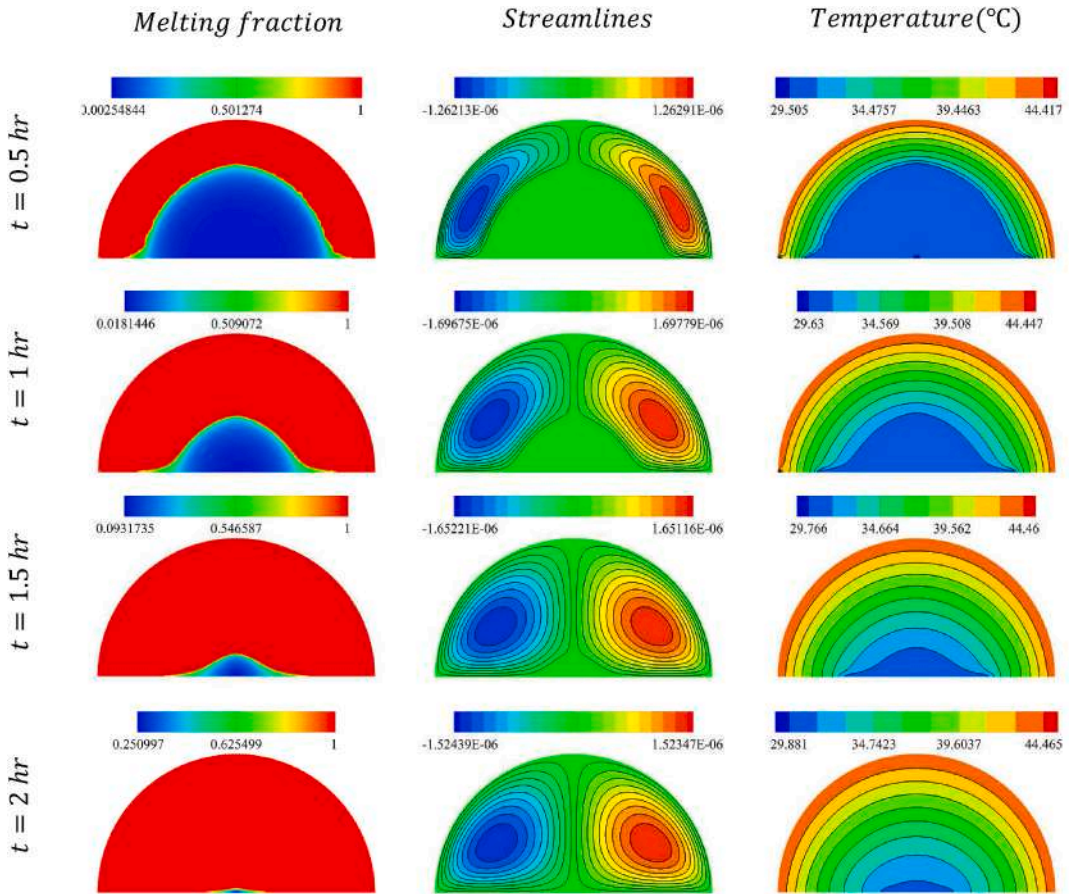
Fig. 7. The melting fraction, streamlines, temperature contours versus time for $\Delta T = 15$, $\varepsilon = 0.95$.
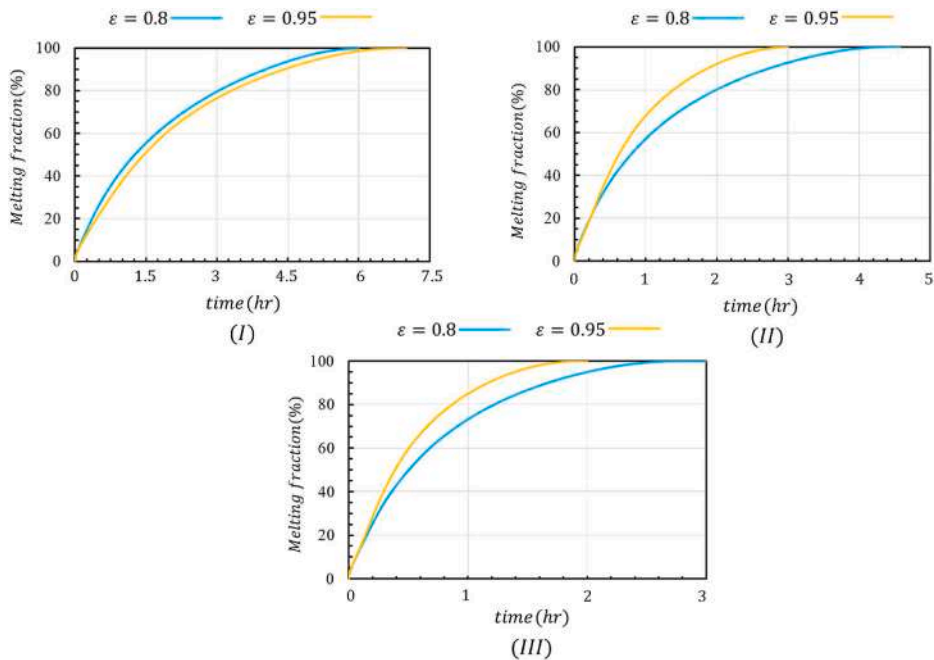

Fig. 8. the melting fraction versus time for I) $\Delta T = 5$, II) $\Delta T = 10$, III) $\Delta T = 15$.

analyzed in following.

First, the effects of porosity are investigated at $\Delta T = 15$. At a constant time, the rising porosity 0.8 to 0.95 enhances the strength of the vortices and the melting fraction (unlike $\Delta T = 5$). Although, the volume of PCM has increased. it can be realized that the effects of convective heat transfer have increased by increasing buoyant force. As a result, the PCM of at porosity 0.95 is molten faster than porosity 0.8. On the other hand, increasing time at porosity 0.95 first increases and then decreases the strength of the vortices. Because at t = 2 h, all PCM has been melted and the after this time, input heat leads to increase PCM temperature, which decreases temperature difference between the surface of the geometry and the flow, and buoyant force.

Now, we compare the effects of temperature difference. In both porosities and at fixed times, the increasing ΔT causes enhance melting fraction for two reasons:

- increasing ΔT leads to increase temperature gradient and heat flux.
- increment ΔT enhances the buoyant force and the strength of the vortices.

Fig. 8 shows the melting fraction versus time to compare the effects and the temperature difference and porosity. Before analyzing the results, it can be said that the volume of PCM in porosity 0.95 is 11.7% higher than $\varepsilon = 0.8$. According to plot (I) in Fig. 8, the rising porosity has no effect on the melting fraction and time, although the volume of PCM has increased by 11.7%. Because the increment of porosity has led to increase strength of flow and convective heat transfer.

Plots II and III in Fig. 8 show that in the first minutes of the melting process, the porosity has no effect on the melting fraction, because the liquid phase flow is very weak and heat is transferred by conductive mechanism. An addition, Increasing the time causes to enhance the buoyant force to move liquid phase, which leads to increase the convective heat transfer to melt the solid PCM. At a fixed time, increasing the porosity from 0.8 to 0.95 increases the melting fraction, although the volume PCM was increased by 11.7%. it can be observed that increment of porosity reduces the Darcy force and increases the convective heat transfer.

6. Conclusion

In the present study, the melting process of paraffin inside a half-cylinder with porous media has been simulated by FVM method, PIMPLE algorithm and regarding effects of free convection for three various temperature difference ($5 < \Delta T < 15$) and two porosities ($\varepsilon = 0.8$, *and* 0.95). Moreover, the porous medium is considered as local thermal non-equilibrium and Darcy model is applied in the momentum equation. Used PCM is a type of paraffin with a melting temperature of $30°C$ and the porous media is made of aluminum metal with pore density 10. The important observations can be listed as below:

- In the $\Delta T = 5, 15$, increasing porosity 0.8 to 0.95 enhances strength of streamlines 123.6%, 161.54% at a fixed time, respectively.
- In all of ΔT, increment of porosity enhances convective heat transfer relative to conductive mechanism in order to enhance the permeability of porous media versus movement of fluid flow.
- In the $\Delta T = 5$, increasing porosity 0.8 to 0.9 increase the volume of PCM 11.7%, but doesn't affect on time of melting process.
- Enhancement of porosity 0.8 to 0.9 rises the volume of PCM 11.7%, and reduces time of melting process 31.7, and 30.8% for $\Delta T = 10$, *and* 15, respectively.
- At the constant porosity 0.8, increment of $\Delta T = 5$ *to* 15 leads to decrease time of melting process 42.3%.
- Melting process behaves as a parabolic with Negative concavity relative to time for all cases.

Author statement

Yan Cao: Supervision, Conceptualization. Hamdi Ayed: Validation, Funding acquisition, Resources. Hussein Togun: Writing - Original Draft, Data Curation. Hajar Alias: Visualization, Investigation. Souhail Mohamed Bouzgarrou: Writing - Review & Editing Makatar Wae-hayee: Project administration, Formal analysis. Riadh Marzouki: Visualization, Writing - Review & Editing.

Declaration of competing interest

The authors declare that they have no known competing financial interests or personal relationships that could have appeared to influence the work reported in this paper.

Acknowledgment

References

[1] S. Ali, S.P. Deshmukh, An overview: applications of thermal energy storage using phase change materials, Mater. Today: Proceedings 26 (2020) 1231–1237.
[2] G. Xiang, Y. Zhang, X. Gao, H. Li, X. Huang, Oblique detonation waves induced by two symmetrical wedges in hydrogen-air mixtures, Fuel 295 (2021) 120615.

[3] Y. Li, D.D. Macdonald, J. Yang, J. Qiu, S. Wang, Point defect model for the corrosion of steels in supercritical water: Part I, film growth kinetics, Corrosion Sci. 163 (2020) 108280.

[4] C. Thirugnanam, S. Karthikeyan, K. Kalaimurugan, Study of phase change materials and its application in solar cooker, Mater. Today: Proceedings 33 (2020) 2890–2896.

[5] H. Zhang, X. Liu, G. Song, H. Yang, Effects of microencapsulated phase change materials on the thermal behavior of multilayer thermal protective clothing, J. Textil. Inst. 112 (6) (2021) 1004–1013.

[6] S. Mondal, Phase change materials for smart textiles–An overview, Appl. Therm. Eng. 28 (11–12) (2008) 1536–1550.

[7] Q. Al-Yasiri, M. Szabó, Incorporation of phase change materials into building envelope for thermal comfort and energy saving: a comprehensive analysis, Journal of Building engineering (2020) 102122.

[8] S.M. Azghandi, M. Weiss, B.D. Arhatari, J. Adrien, E. Maire, M.R. Barnett, A rationale for the influence of grain size on failure of magnesium alloy AZ31: an in situ X-ray microtomography study, Acta Mater. 200 (2020) 619–631.

[9] B. Hu, Y. Wu, H. Wang, Y. Tang, C. Wang, Risk mitigation for rockfall hazards in steeply dipping coal seam: a case study in Xinjiang, northwestern China, Geomatics, Nat. Hazards Risk 12 (1) (2021) 988–1014.

[10] Shu-Rong Yan,Hazim Moria, Samira Pourhedayat, Mehran Hashemian, Soheil Asaadi, Hamed Sadighi Dizaji, Kittisak Jermsittiparsert, A critique of effectiveness concept for heat exchangers; theoretical-experimental study, Int. J. Heat Mass Tran. 159, 2020, 120160.

[11] N. Wu, X. Zhou, P. Kidkhunthod, W. Yao, T. Song, Y. Tang, K-Ion Battery Cathode Design Utilizing Trigonal Prismatic Ligand Field. Advanced Materials, 2021, p. 2101788.

[12] B. Ji, W. Yao, Y. Zheng, P. Kidkhunthod, X. Zhou, S. Tunmee, S. Sattayaporn, H.M. Cheng, H. He, Y. Tang, A fluoroxalate cathode material for potassium-ion batteries with ultra-long cyclability, Nat. Commun. 11 (1) (2020) 1–10.

[13] J. Qiu, D. Huo, Y. Xia, Phase-change materials for controlled release and related applications, Adv. Mater. 32 (25) (2020) 2000660.

[14] Z. Liu, C. Ma, Numerical analysis of melting with constant heat flux heating in a thermal energy storage system, Energy Convers. Manag. 43 (18) (2002) 2521–2538.

[15] S. Rostami, M. Afrand, A. Shahsavar, M. Sheikholeslami, R. Kalbasi, S. Aghakhani, M.S. Shadloo, H.F. Oztop, A review of melting and freezing processes of PCM/ nano-PCM and their application in energy storage, Energy 211 (2020) 118698.

[16] X. Zhang, Y. Tang, F. Zhang, C.S. Lee, A novel aluminum–graphite dual-ion battery, Advanced Energy Materials 6 (11) (2016) 1502588.

[17] G. Xiao, K. Song, Y. He, W. Wang, Y. Zhang, W. Dai, Prediction and experimental research of abrasive belt grinding residual stress for titanium alloy based on analytical method, Int. J. Adv. Manuf. Technol. (2021) 1–15.

[18] T. Li, Z. Dai, M. Yu, W. Zhang, Numerical investigation on the aerodynamic resistances of double-unit trains with different gap lengths, Engineering Applications of Computational Fluid Mechanics 15 (1) (2021) 549–560.

[19] X. Li, X. Sheng, Y. Guo, X. Lu, H. Wu, Y. Chen, L. Zhang, J. Gu, Multifunctional HDPE/CNTs/PW composite phase change materials with excellent thermal and electrical conductivities, J. Mater. Sci. Technol. 86 (2021) 171–179.

[20] D. Ürge-Vorsatz, L.F. Cabeza, S. Serrano, C. Barreneche, K. Petrichenko, Heating and cooling energy trends and drivers in buildings, Renew. Sustain. Energy Rev. 41 (2015) 85–98.

[21] A. Ghosh, S. Neogi, Effect of fenestration geometrical factors on building energy consumption and performance evaluation of a new external solar shading device in warm and humid climatic condition, Sol. Energy 169 (2018) 94–104.

[22] Z. Xu, X. Qiao, K. Sun, Environmental-friendly corn stover/poly (butylene adipate-co-terephthalate) biocomposites, Materials Today Communications 25 (2020) 101541.

[23] C. Liu, X. Gao, D. Chi, Y. He, M. Liang, H. Wang, On-line chatter detection in milling using fast kurtogram and frequency band power, Eur. J. Mech. Solid. (2021) 104341.

[24] .

[25] M. Jalili, A. Chitsaz, M. Hashemian, M.A. Rosen, Economic and environmental assessment using emergy of a geothermal power plant, Energy Convers. Manag. 228 (2021) 113666.

[26] S. Jafary, S. Khalilarya, A. Shawabkeh, M. Wae-hayee, M. Hashemian, A complete energetic and exergetic analysis of a solar powered trigeneration system with two novel organic Rankine cycle (ORC) configurations, J. Clean. Prod. 281 (2021) 124552.

[27] Y. Cao, H. Ayed, S. Jafarmadar, M.A.A. Abdollahi, A. Farag, M. Wae-hayee, M. Hashemian, PEM fuel cell cathode-side flow field design optimization based on multi-criteria analysis of liquid-slug dynamics, J. Ind. Eng. Chem. 98 (2021) 397–412.

[28] C. Liu, M. Hashemian, A. Shawabkeh, H.S. Dizaji, S. Saleem, M.F.M. Batcha, M. Wae-hayee, CFD-based irreversibility analysis of avant-garde semi-O/O-shape grooving fashions of solar pond heat trade-off unit, Renew. Energy 171 (2021) 328–343.

[29] Y. Cao, H. Ayed, M. Hashemian, A. Issakhov, M. Wae-hayee, Thermal/frictional performance of spiral pipe with ring-shape depression used as in-pond heat exchanger, Sol. Energy 224 (2021) 742–756.

[30] Yan Cao, Mohammad AliAbdous, Shahriyar Ghazanfari Holagh, Mahmood Shafiee, Mehran Hashemian, Entropy generation and sensitivity analysis of R134a flow condensation inside a helically coiled tube-in-tube heat exchanger, Int. J. Refrig., Available online 8 June 2021. https://doi.org/10.1016/j.ijrefrig.2021.06. 007.

[31] M. Aliakbari, Numerical investigation of heat transfer of nanofluids in a channel under the influence of porous area, J. Fund. Appl. Sci. 9 (2017) 1175–1188.

[32] S.M.M.J. Sarayi, A. Bahrami, M.N. Bahrami, Free vibration and wave power reflection in Mindlin rectangular plates via exact wave propagation approach, Compos. B Eng. 144 (2018) 195–205.

[33] P. Patel, S.M.M.J. Sarayia, D. Chen, A.L. Hammond, R.J. Damiano, J.M. Davies, J. Xu, H. Meng, Fast virtual coiling algorithm for intracranial aneurysms using pre-shape path planning, Comput. Biol. Med. (2021) 104496.

[34] M.S. Sadrabadi, M. Hedayat, I. Borazjani, A. Arzani, Fluid-structure coupled biotransport processes in aortic valve disease, J. Biomech. 117 (2021) 110239.

[35] M. Habibi, S. Dawson, A. Arzani, Data-driven pulsatile blood flow physics with dynamic mode decomposition, Fluid 5 (3) (2020) 111.

[36] M. Habibi, R.M. D'Souza, S.T. Dawson, A. Arzani, Integrating multi-fidelity blood flow data with reduced-order data assimilation, Comput. Biol. Med. (2021) 104566.

[37] S.S. Meschi, A. Farghadan, A. Arzani, Flow topology and targeted drug delivery in cardiovascular disease, J. Biomech. 119 (2021) 110307.

[38] S. Jafarzadeh, A.N. Sadr, E. Kaffash, S. Goudarzi, E. Golab, A. Karimipour, The effect of hematocrit and nanoparticles diameter on hemodynamic parameters and drug delivery in abdominal aortic aneurysm with consideration of blood pulsatile flow, Comput. Methods Progr. Biomed. 195 (2020) 105545.

[39] M. Abbasi, A.N. Esfahani, E. Golab, O. Golestanian, N. Ashouri, S.M. Sajadi, F. Ghaemi, D. Baleanu, A. Karimipour, Effects of brownian motions and thermophoresis diffusions on the hematocrit and LDL concentration/diameter of pulsatile non-Newtonian blood in abdominal aortic aneurysm, J. Non-Newtonian Fluid Mech. (2021) 104576.

[40] S.M.M.J. Sarayi, R.J. Damiano, P. Patel, G. Dargush, A.H. Siddiqui, H. Meng, A Nonlinear Mechanics-Based Virtual Coiling Method for Intracranial Aneurysm, 2020 arXiv preprint arXiv:2009.05592.

[41] S.Y. Motlagh, E. Golab, A.N. Sadr, Two-phase modeling of the free convection of nanofluid inside the inclined porous semi-annulus enclosure, Int. J. Mech. Sci. 164 (2019) 105183.

[42] S. Goudarzi, M. Shekaramiz, A. Omidvar, E. Golab, A. Karimipour, A. Karimipour, Nanoparticles migration due to thermophoresis and Brownian motion and its impact on Ag-MgO/Water hybrid nanofluid natural convection, Powder Technol. 375 (2020) 493–503.

[43] E. Golab, S. Goudarzi, H. Kazemi-Varnamkhasti, H. Amigh, F. Ghaemi, D. Baleanu, A. Karimipour, Investigation of the effect of adding nano-encapsulated phase change material to water in natural convection inside a rectangular cavity, Journal of Energy Storage 40 (2021) 102699.

[44] Z. Badiei, M. Eslami, K. Jafarpur, Performance improvements in solar flat plate collectors by integrating with phase change materials and fins: a CFD modeling, Energy 192 (2020) 116719.

[45] M.A. Gómez, M.A. Álvarez Feijoo, R. Comesaña, P. Eguía, J.L. Míguez, J. Porteiro, CFD simulation of a concrete cubicle to analyze the thermal effect of phase change materials in buildings, Energies 5 (7) (2012) 2093–2111.

[46] P. Talebizadeh Sardari, G.S. Walker, M. Gillott, D. Grant, D. Giddings, Numerical modelling of phase change material melting process embedded in porous media: effect of heat storage size, Proc. IME J. Power Energy 234 (3) (2020) 365–383.

[47] Yusuf A. Al-Turki, Hazim Moria, Ali Shawabkeh, Samira Pourhedayat, Mehran Hashemian, Hamed Sadighi Dizaji, Thermal, frictional and exergetic analysis of non-parallel configurations for plate heat exchangers, Chemical Engineering and Processing - Process Intensification 161 (2021), https://doi.org/10.1016/j.cep.2021.108319, 108319.

[48] Samira Pourhedayat, Seyed Mehdi Pesteei, Hamed Ebrahimi Ghalinghie, Mehran Hashemian, Muhammad Aqeel Ashraf, Thermal-exergetic behavior of triangular vortex generators through the cylindrical tubes, Int. J. Heat Mass Tran. 151 (2020), https://doi.org/10.1016/j.ijheatmasstransfer.2020.119406, 119406.

[49] Yan Cao, Hamdi Ayed, Hamed Sadighi Dizaji, Mehran Hashemian, Makatar Wae-hayee, Entropic analysis of a double helical tube heat exchanger including circular depressions on both inner and outer tube, Case Studies in Thermal Engineering 26 (2021), https://doi.org/10.1016/j.csite.2021.101053, 101053.

[50] S. Rahman, S. Issa, Z. Said, M.E.H. Assad, R. Zadeh, Y. Barani, Performance enhancement of a solar powered air conditioning system using passive techniques and SWCNT/R-407c nano refrigerant, Case Studies in Thermal Engineering 16 (2019) 100565.

[51] A. Ahmadi, M.A. Ehyaei, A. Doustgani, M.E.H. Assad, A. Hmida, D.H. Jamali, R. Kumar, Z.X. Li, A. Razmjoo, Recent residential applications of low-temperature solar collector, J. Clean. Prod. 279 (2021) 123549.

[52] K.G. Kumar, E.H.B. Hani, M.E.H. Assad, M. Rahimi-Gorji, S. Nadeem, A novel approach for investigation of heat transfer enhancement with ferromagnetic hybrid nanofluid by considering solar radiation, Microsyst. Technol. 27 (1) (2021) 97–104.

[53] A. Khosravi, S. Syri, X. Zhao, M.E.H. Assad, An artificial intelligence approach for thermodynamic modeling of geothermal based-organic Rankine cycle equipped with solar system, Geothermics 80 (2019) 138–154.

[54] A.S. Rad, A. Shadravan, A.A. Soleymani, N. Motaghedi, Lewis acid-base surface interaction of some boron compounds with N-doped graphene; first principles study, Curr. Appl. Phys. 15 (10) (2015) 1271–1277.

[55] A. Shokrolahzade Tehrani, A. Shadravan, M. Kashefi Asl, Investigation of kinetics and isotherms of boron adsorption of water samples by natural clinoptilolite and clinoptilolite modified with sulfuric acid, Nashrieh Shimi va Mohandesi Shimi Iran 35 (4) (2017) 21–32.

[56] A. Shadravan, P.S. Goh, A.F. Ismail, Nanomaterials for pressure retarded osmosis, Advances in Water Desalination Technologies (2021) 583–618.

[57] H.J. Xu, L. Gong, C.Y. Zhao, Y.H. Yang, Z.G. Xu, Analytical considerations of local thermal non-equilibrium conditions for thermal transport in metal foams, Int. J. Therm. Sci. 95 (2015) 73–87.

[58] B. Kamkari, H. Shokouhmand, F. Bruno, Experimental investigation of the effect of inclination angle on convection-driven melting of phase change material in a rectangular enclosure, Int. J. Heat Mass Tran. 72 (2014) 186–200.

[59] M. Eslami, M.A. Bahrami, Sensible and latent thermal energy storage with constructal fins, Int. J. Hydrogen Energy 42 (28) (2017) 17681–17691.

[60] Yan Cao, Hamdi Ayed, Mehran Hashemian, Alibek Issakhov, Fahd Jarad, Makatar Wae-hayee, Inducing swirl flow inside the pipes of flat-plate solar collector by using multiple nozzles for enhancing thermal performance, Renew. Energy 180 (2021) 1344–1357, https://doi.org/10.1016/j.renene.2021.09.018.